2004-04-28

On Noncoherent Detection of CPM

Michael D. Rice
mdr@byu.edu

Erik Perrins

On Noncoherent Detection of CPM

Erik Perrins*, *Student Member, IEEE*, and Michael Rice, *Senior Member, IEEE*
Department of Electrical and Computer Engineering
Brigham Young University
Provo, UT 84602
847.697.3378 (Voice)
801.422.0201 (Fax)
esp@ee.byu.edu

Abstract — It is well understood that the performance of noncoherent receivers with multi-symbol observation intervals approaches that of coherent receivers as the observation interval grows arbitrarily large. However, since complexity also grows exponentially with observation length, there are practical limits to this approach. In this paper we present a noncoherent receiver for continuous phase modulation (CPM) whose structure is a hybrid between existing coherent and noncoherent receiver architectures. The presentation is given in the most general M-ary multi-h terms, with some emphasis on the special and popular case of single-h CPM. The receiver has a multi-symbol observation parameter similar to that of existing noncoherent receivers. However, it uses a recursive metric similar to that of the optimal coherent receiver, which allows it to use much smaller values of the multi-symbol observation parameter thus reducing the required complexity. We analyze the performance of this receiver over the noncoherent additive white Gaussian noise (AWGN) channel and derive a union bound on the bit error probability. We confirm the usefulness of the bound with computer simulations. We also give thorough examples using quaternary raised cosine (RC) single- and multi-h CPM schemes. With these examples we show that previous noncoherent CPM techniques extend to the general multi-h case. The simulations also show that the proposed receiver outperforms these other noncoherent techniques, at a fraction of the complexity.

*corresponding author

1 Introduction

Continuous Phase Modulation (CPM) is in wide use for its attractive power and bandwidth properties. However, CPM detectors often suffer from high implementation complexity in terms of the required number of correlators (matched filters) and trellis states. Another difficulty with CPM is receiver synchronization. One means of avoiding some of the burden of synchronization, namely carrier phase recovery, is the use noncoherent detection techniques, which is the focus of this paper.

There are numerous noncoherent detection techniques that have been proposed, a thorough summary of these is found in [1, 2]. Of these is the class of detectors with multiple-symbol observation intervals. Generally speaking, the performance of multi-symbol noncoherent detection schemes approaches that of coherent detection as the observation interval (and complexity) grows arbitrarily large. This was first found in [3] for CPM and has been confirmed in [2, 4, 5] to name a few.

A key assumption in multi-symbol noncoherent detectors is that the carrier phase, while unknown, varies slowly enough that it can be assumed to remain constant over a multi-symbol observation interval. This allows receiver metrics to combine constructively over this interval. By contrast, the optimal coherent receiver removes the carrier phase so that receiver metrics combine constructively over indefinitely long observation intervals, which leads to an efficient recursive implementation via the Viterbi algorithm.

In this paper we present a noncoherent receiver that is a hybrid of coherent and noncoherent architectures. We describe this receiver in the most general terms using the multi-h CPM model, with equal applicability to the more common special case of single-h CPM. The receiver has a multi-symbol observation parameter, N, which is similar to that of existing noncoherent receivers. A key feature of the receiver is that it has a recursive metric which is similar to the optimal coherent receiver. The difference is that the cumulative metric $\lambda(n)$ is a "leaky" integral, i.e. $\lambda(n) = a\lambda(n-1) + z(n)$, where $z(n)$ is a metric increment and the *leakage coefficient* a is in the range $0 \leq a < 1$ (by contrast, the cumulative metric in the coherent case has $a = 1$ and is not a leaky integral). This cumulative metric partially achieves the performance gain of an infinitely long

observation interval without requiring large values of N. This is significant since the increments of N come with exponential increases in complexity.

We analyze the performance of this receiver over the noncoherent AWGN channel. We derive the exact pairwise error probability, which in turn is used to obtain a union bound on the bit error probability. We also use an approximation to obtain an equivalent minimum Euclidian distance which gives a convenient single-parameter characterization of error performance.

In the next section we describe the various detection techniques for multi-h CPM, including the proposed noncoherent technique (in doing so, we also show that these existing techniques extend to the multi-h case). In Section 3 we derive the pairwise error probability of this new noncoherent technique and show how to evaluate the overall bit error probability. We give examples in Section 4 using quaternary single- and multi-h RC signaling schemes and offer conclusions in Section 5.

2 Detection of CPM

2.1 Signal Model

The complex-baseband representation of the multi-h CPM signal, following standard notation [6], is given by

$$s(t,\boldsymbol{\alpha}) = \sqrt{\frac{\mathcal{E}}{T}}\exp\big(j\psi(t,\boldsymbol{\alpha})\big) \tag{1}$$

$$\psi(t,\boldsymbol{\alpha}) = 2\pi\sum_{i=-\infty}^{n}\alpha_i h_{\underline{i}} q(t-iT), \qquad nT \le t < (n+1)T \tag{2}$$

where $\mathcal{E}$ is the symbol energy, T is the symbol duration, $\{h_{\underline{i}}\}$ is the set of N_h modulation indexes, $\boldsymbol{\alpha} = \{\alpha_i\}$ are the information symbols in the M-ary alphabet $\{\pm 1, \pm 3, \cdots, \pm(M-1)\}$, and $q(t)$ is the phase pulse. In this paper, the underlined subscript notation in (2) is defined as modulo-N_h, i.e. $\underline{i} \triangleq i \bmod N_h$. We assume the modulation indexes are rational numbers of the form

$$h_{\underline{i}} = 2k_{\underline{i}}/p \tag{3}$$

where $k_{\underline{i}}$ and p are relatively prime integers. The phase pulse $q(t)$ and the frequency pulse $f(t)$ are related by

$$q(t) = \int_0^t f(\tau)\, d\tau. \tag{4}$$

The frequency pulse is supported over the time interval $(0, LT)$ (it is zero otherwise) and is subject to the constraint

$$\int_0^{LT} f(\tau)\, d\tau = q(LT) = \frac{1}{2}. \tag{5}$$

In light of the constraints on $f(t)$ and $q(t)$, Equation (2) can be written as

$$\begin{aligned}\psi(t, \boldsymbol{\alpha}) &= 2\pi \sum_{i=n-L+1}^{n} \alpha_i h_{\underline{i}} q(t - iT) + \left(\pi \sum_{k=-\infty}^{n-L} \alpha_k h_{\underline{k}} \right) \bmod 2\pi. \\ &= \theta(t, \boldsymbol{\alpha}_n) + \theta_n \end{aligned} \tag{6}$$

The term $\theta(t, \boldsymbol{\alpha}_n)$ is a function of the *correlative state vector* $\boldsymbol{\alpha}_n = (\alpha_{n-L+1}, \alpha_{n-L+2}, \cdots, \alpha_n)$, which contains the L symbols being modulated by the phase pulse. Due to (3), the *phase state* θ_n takes on p distinct values $0, 2\pi/p, 2 \cdot 2\pi/p, \ldots, (p-1)2\pi/p$.

The model for the received complex-baseband signal is

$$r(t) = s(t, \boldsymbol{\alpha}) e^{j\phi(t)} + n(t) \tag{7}$$

where $n(t) = x(t) + jy(t)$ is complex-valued additive white Gaussian noise with zero-mean and single-sided power spectral density N_0. The phase shift $\phi(t)$ introduced by the channel is unknown in general.

2.2 Coherent Detection

For coherent detection, the receiver has perfect knowledge of $\phi(t)$, where we assume $\phi(t) = 0$ with no loss in generality. The objective of the coherent receiver is to maximize the likelihood function [6]

$$\Lambda(\boldsymbol{\alpha}) \sim -\int \big(r(t) - s(t, \boldsymbol{\alpha})\big)^2\, dt \tag{8}$$

which comes from the AWGN assumption. Maximizing (8) is equivalent to using the decision rule

$$\hat{\boldsymbol{\alpha}} = \arg\max_{\tilde{\boldsymbol{\alpha}}} \mathrm{Re} \int r(t) s^*(t, \tilde{\boldsymbol{\alpha}})\, dt \tag{9}$$

where $\hat{\boldsymbol{\alpha}}$ is the receiver output and $\tilde{\boldsymbol{\alpha}}$ is a hypothesized data sequence. Using (6) we can partition the hypothesis into a correlative state vector and a phase state. We refer to the l-th possible value of the correlative state vector as

$$\tilde{\boldsymbol{\alpha}}_n^l = (\tilde{\alpha}_{n-L+1}^l, \tilde{\alpha}_{n-L+2}^l, \cdots, \tilde{\alpha}_n^l), \qquad 0 \le l < M^L \tag{10}$$

where the index l enumerates all the M^L possible combinations of values that the coordinates α_n^l etc. can assume. The m-th value of the phase state is given by

$$\tilde{\theta}_n^m = \left(\pi \sum_{k=-\infty}^{n-L} \tilde{\alpha}_k^m h_{\underline{k}} \right) \bmod 2\pi = \frac{2\pi}{p} m, \qquad 0 \le m < p. \tag{11}$$

The trellis for this receiver has $S = pM^{L-1}$ states, with M branches at each state. Each branch in the trellis is associated with an (l, m) pair which specifies the hypothesis along that branch. We note that the phase state allows the receiver to maintain an infinitely long hypothesis with only a finite number of states. We can compute (9) recursively using the metric

$$\lambda^{l,m}(n) = \lambda^{l,m}(n-1) + \mathrm{Re}\{ z^l(n) e^{-j\tilde{\theta}_n^m} \} \tag{12}$$

where the sampled matched filter output $z^l(n)$ is defined as

$$z^l(n) = \sqrt{\frac{1}{T}} \int_{nT}^{(n+1)T} r(\tau) e^{-j\theta(\tau, \tilde{\alpha}_n^l)}\, d\tau. \tag{13}$$

The computation of (12) is efficiently performed using the Viterbi algorithm. Each of the branch metrics are computed and the surviving path at each merging node is the one with the largest metric. At each time step, the receiver traces back along the path with the largest overall metric to some

traceback length D and outputs the symbol $\hat{\alpha}_{n-D}$. The information required to force $\phi(t) = 0$ is provided by a carrier phase estimator (see [7] and references therein).

2.3 Noncoherent Detection

For noncoherent detection, the receiver requires no knowledge of $\phi(t)$ and thus avoids the additional complexity needed to estimate the carrier phase; however, most noncoherent techniques (including the one presented here) assume $\phi(t)$ is slowly varying such that it is assumed to be constant (i.e. $\phi(t) = \phi$) over a brief period of time and is uniformly distributed over the interval $[0, 2\pi)$. Unfortunately, this assumption does not always hold in a practical setting. Thus, as the conclusion in [3] states, noncoherent receivers must have a means of "forgetting" or otherwise coping with past observations that inevitably become inconsistent with present observations.

The likelihood function for the received signal in (7), averaged over ϕ, is given by [8]

$$\Lambda(\boldsymbol{\alpha}) \sim I_0\left(\frac{1}{\sigma^2}\left|\int r(t)s^*(t,\boldsymbol{\alpha})\,dt\right|\right) \tag{14}$$

where $I_0(\cdot)$ is the zeroth order modified Bessel function of the first kind. This likelihood function is much simplified from its full form in [8] due to the constant envelope of (1). Maximizing (14) is equivalent to maximizing the argument of $I_0(\cdot)$, which suggests the decision rule

$$\hat{\boldsymbol{\alpha}} = \arg\max_{\tilde{\boldsymbol{\alpha}}}\left|\int r(t)s^*(t,\tilde{\boldsymbol{\alpha}})\,dt\right|^2. \tag{15}$$

We note that the decision rules in (9) and (15) are identical except that the coherent receiver takes the real part of the correlation and the noncoherent receiver takes the magnitude-squared of the correlation.

For noncoherent receivers, we consider a hypothesis containing the correlative state vector in (10), and the *rotational state vector* $\boldsymbol{\beta}_n^m$, defined as

$$\tilde{\boldsymbol{\beta}}_n^r = (\tilde{\alpha}_{n-L-N+2}^r, \tilde{\alpha}_{n-L-N+3}^r, \cdots, \tilde{\alpha}_{n-L}^r), \qquad 0 \le r < M^{N-1} \tag{16}$$

where the length of the rotational state vector is parameterized by the integer $N > 0$. The rotational state vector is associated with a *branch phase* $\Omega(\tilde{\boldsymbol{\beta}}_n^r)$ which is given by

$$\Omega(\tilde{\boldsymbol{\beta}}_n^r) = \left(\pi \sum_{k=n-L-N+2}^{n-L} \tilde{\alpha}_k^r h_{\underline{k}} \right) \bmod 2\pi. \tag{17}$$

The trellis associated with this hypothesis has $S = M^{L+N-2}$ states, where each branch in the trellis is associated with an (l, r) pair that specifies the branch hypothesis. We note that this trellis has only a finite hypothesis, since we have removed the phase state and replaced it with the $N-1$ symbol coordinates in $\tilde{\boldsymbol{\beta}}_n^r$. We also observe that as N increases, the branch phase in (17) approximates the phase state in (11), at the expense of exponentially increasing complexity. We consider three receiver schemes that use this noncoherent trellis.

In terms of the above quantities, the noncoherent receiver in [3] uses the complex-valued metric

$$\begin{aligned} \lambda^{l,r}(n) &= \sum_{k=n-N_1+1}^{n+N_2} z^l(k) e^{-j\Omega(\tilde{\boldsymbol{\beta}}_k^r)} & (18) \\ &= \lambda^{l,r}(n-1) + z^l(n+N_2) e^{-j\Omega(\tilde{\boldsymbol{\beta}}_{n+N_2}^r)} - z^l(n-N_1) e^{-j\Omega(\tilde{\boldsymbol{\beta}}_{n-N_1}^r)} & (19) \end{aligned}$$

where $N_1 + N_2 - 1 = N$. There is no traceback operation in this receiver; the receiver simply computes the metrics for each branch, selects the survivor at each merging node with the largest metric (in the magnitude-squared sense), and outputs the symbol $\hat{\alpha}_n$ corresponding to the hypothesis which maximizes (19) over all the states. There is an implied delay of N_2 needed in order to compute these metrics. From (19) it is obvious how this receiver forgets past observations, since the newest observation in the length-N window is added in and the oldest observation is subtracted out. A drawback with this receiver is that a large value of N (say $N \approx 10$) is often required to achieve signal distances which are comparable to that of the coherent receiver [3]. This is particularly true for more complex CPM schemes, such as nonbinary and partial response schemes.

The noncoherent receiver metrics in [2] are obtained by expanding the magnitude-squared expression in (15) and keeping only those terms which are relevant to the hypothesis, yielding the

recursive metric

$$\lambda^{l,r}(n) = \lambda^{l,r}(n-1) + \text{Re} \sum_{k=1}^{N-1} z^l(n) e^{-j\Omega(\tilde{\boldsymbol{\beta}}_n^r)} \left[z^l(n-k) e^{-j\Omega(\tilde{\boldsymbol{\beta}}_{n-k}^r)} \right]^*. \tag{20}$$

We note that the presentation in [2] uses matched filters which are based on the pulse amplitude modulation (PAM) representation of CPM [9, 10] and are not the same as (13). For the purposes of our discussion, the metric in (20) is still valid; however the PAM representation does result in additional complexity savings. The metric increment in (20) is simply the most recent matched filter output correlated against the $N-1$ previous matched filter outputs (all of the matched filter outputs are phase-rotated by the branch phase in order to be consistent with the particular hypothesis). By correlating past observations with the most recent one, these metrics "adjust" themselves according to the present value of the channel phase in the event that $\phi(t)$ is changing. This receiver uses a traditional traceback operation. Also, since (20) is real-valued, there is no magnitude-squared operation required in determining the survivors at each merging node. There is no analysis that describes the performance of this receiver; however, the simulations in [2] show that near-optimal performance can be achieved with $N \leq 5$.

Using (15) as motivation, we propose the complex-valued recursive metric

$$\lambda^{l,r}(n) = a\lambda^{l,r}(n-1) + z^l(n) e^{-j(\Omega(\tilde{\boldsymbol{\beta}}_n^r) + \hat{\theta}_n^{l,r})} \tag{21}$$

which is similar to the recursive metric of the optimal coherent receiver in (12). The branch metric increments are simply the sampled matched filter output rotated by a certain phase such that it is consistent with the ongoing hypothesis of the particular trellis path. However, the *leakage factor* a, where $0 \leq a < 1$, causes the cumulative metric $\lambda^{l,r}(n)$ to be a leaky integral with limited memory, which is the means by which this receiver "forgets" past observations. The phase rotation in (21) is divided into two parts, the branch phase in (17) and the *cumulative phase* $\hat{\theta}_n^{l,r}$, which is given by

$$\hat{\theta}_n^{l,r} = \left(\pi \sum_{k=-\infty}^{n-L-N+1} \hat{\alpha}_k^{l,r} h_{\underline{k}} \right) \bmod 2\pi. \tag{22}$$

This cumulative phase is not composed of *hypothesized* data symbols; instead, it is the phase contribution of the history of past *decisions*, $\hat{\alpha}_k^{l,r}$, that have been made in the trellis. Each state in the trellis maintains a value for the cumulative phase (just as they also maintain a cumulative metric) and it is updated recursively and propagated with the surviving metric at each merging node. Similar applications using decision feedback have been successfully applied to CPM [11]. The branch metrics in (21) propagate from state to state as complex numbers; however, when competing metrics are compared to each other at merges, the survivor is the one with the largest magnitude squared, as indicated by (15).

In summary, this receiver is similar to the optimal coherent CPM receiver. For the coherent case, the phase state in (11) fills the role that is here shared by the branch and cumulative phases. Also, since the coherent receiver forces $\phi = 0$, only the real part of the cumulative metric is needed in that case. As time unfolds, the metric for the correct path in the coherent receiver grows without bound along the positive real axis. Here, the metric of the correct path lies in the complex plane and grows away from the origin at an unknown angle of ϕ and reaches a magnitude, in the limit, of $\sqrt{\mathcal{E}}/(1-a)$.

Like the two other multi-symbol noncoherent receivers we have summarized, there is a means (via the parameter N) of increasing the number of symbols in the receiver hypothesis to an arbitrarily large number. This approximates the role of the phase state in the coherent receiver, which cannot be used here since the magnitude-squared comparison of the metrics destroys the information that distinguishes the different phase states from each other.

As we shall see in later sections, the role of the leakage factor is to strike a balance between helping the correct path maintain distance from competing paths, while at the same time allowing a way for the negative impact of previous incorrect decisions and channel phase variations to fade away. The receiver *complexity* is not linked to the presence of the cumulative metric (or the leakage factor) in any way, since the number of states is simply $S = M^{L+N-2}$; however, in the following sections we shall see that the leakage factor does play a role in receiver *performance*, by way of the equivalent signal distance which we derive next.

3 Performance Analysis

3.1 Pairwise Error Probability

We seek the quantity $P(\boldsymbol{\alpha}_i \rightarrow \boldsymbol{\alpha}_j)$, which is the probability of the receiver choosing the sequence $\boldsymbol{\alpha}_j$ given $\boldsymbol{\alpha}_i$ is transmitted. We begin by writing (21) as

$$Z_i(n) = \sum_{k=-\infty}^{n} a^{n-k} z_i(k) \tag{23}$$

where we redefine the matched filter output in (13) as

$$z_i(k) = \int_{kT}^{(k+1)T} r(\tau) e^{-j\psi(\tau, \boldsymbol{\alpha}_i)}\, d\tau \tag{24}$$

having absorbed the branch and cumulative phases back into $\psi(\tau, \boldsymbol{\alpha})$ as they are in (2). A similar definition can be made for Z_j. In this analysis we do not account for any additional errors introduced by the decision feedback in (22). The effects of decision feedback will be evaluated in the simulations, as was also done in [11]. With these definitions and assumptions in place, the pairwise error probability is simply

$$P(\boldsymbol{\alpha}_i \rightarrow \boldsymbol{\alpha}_j) = Pr\big\{|Z_i(n)|^2 < |Z_j(n)|^2\big\} = Pr\big\{|Z_i(n)| < |Z_j(n)|\big\}. \tag{25}$$

For the complex Gaussian random variables $Z_i(n)$ and $Z_j(n)$, whose variances are equal, this probability has been shown to be [12]

$$P(\boldsymbol{\alpha}_i \rightarrow \boldsymbol{\alpha}_j) = \frac{1}{2}\big[1 - Q(\sqrt{B}, \sqrt{A}) + Q(\sqrt{A}, \sqrt{B})\big] \tag{26}$$

where $Q(x, y)$ is Marcum's Q-function [13] and

$$\begin{aligned} B &= \frac{1}{\sigma^2}\left[\frac{|M_i|^2 + |M_j|^2 - 2|\rho||M_i||M_j|\cos(\theta_i - \theta_j + \theta_\rho)}{1 - |\rho|^2} + \frac{|M_i|^2 - |M_j|^2}{\sqrt{1 - |\rho|^2}}\right] \\ A &= \frac{1}{\sigma^2}\left[\frac{|M_i|^2 + |M_j|^2 - 2|\rho||M_i||M_j|\cos(\theta_i - \theta_j + \theta_\rho)}{1 - |\rho|^2} - \frac{|M_i|^2 - |M_j|^2}{\sqrt{1 - |\rho|^2}}\right] \end{aligned} \tag{27}$$

The quantities in the above expressions are defined as

$$\begin{aligned} M_i &= E\{Z_i\}, \qquad M_j = E\{Z_j\} && (28)\\ \sigma^2 &= E\{Z_i^* Z_i\} = E\{Z_j^* Z_j\} && (29)\\ \rho &= \frac{1}{\sigma^2} E\{(Z_i - M_i)^*(Z_j - M_j)\} && (30)\\ \theta_i &= \angle M_i, \qquad \theta_j = \angle M_j, \qquad \theta_\rho = \angle \rho. && (31) \end{aligned}$$

Our task is to evaluate these quantities based on (23). From (7) and (24) we have

$$\begin{aligned} M_i &= \frac{\sqrt{\mathcal{E}}}{T} \sum_{k=-\infty}^{n} a^{n-k} \int_{kT}^{(k+1)T} e^{j(\psi(\tau,\boldsymbol{\alpha}_i)+\phi)} e^{-j\psi(\tau,\boldsymbol{\alpha}_i)}\, d\tau = \frac{\sqrt{\mathcal{E}} e^{j\phi}}{1-a} && (32)\\ M_j &= \frac{\sqrt{\mathcal{E}}}{T} \sum_{k=-\infty}^{n} a^{n-k} \int_{kT}^{(k+1)T} e^{j(\psi(\tau,\boldsymbol{\alpha}_i)+\phi)} e^{-j\psi(\tau,\boldsymbol{\alpha}_j)}\, d\tau = \sqrt{\mathcal{E}} e^{j\phi} \delta_a && (33) \end{aligned}$$

where

$$\delta_x = \frac{1}{T} \sum_{k=-\infty}^{n} x^{n-k} \int_{kT}^{(k+1)T} e^{j\psi(\tau,\boldsymbol{\gamma})}\, d\tau \tag{34}$$

which is a function only of the difference between the two data sequences $\boldsymbol{\gamma} = \boldsymbol{\alpha}_i - \boldsymbol{\alpha}_j$. For the variance we have

$$\sigma^2 = E\left\{ \frac{1}{T} \left| \sum_{k=-\infty}^{n} a^{n-k} \int_{kT}^{(k+1)T} n(\tau) e^{-j\psi(\tau,\boldsymbol{\alpha}_i)}\, d\tau \right|^2 \right\} = \frac{N_0}{1-a^2} \tag{35}$$

and for the covariance

$$\begin{aligned} \rho = \frac{1}{\sigma^2 T} &\sum_{k=-\infty}^{n} \sum_{m=-\infty}^{n} a^{2n-k-m} \\ &\times \int_{kT}^{(k+1)T} \int_{mT}^{(m+1)T} E\{n(\tau_1) n(\tau_2)\} e^{-j\psi(\tau_1,\boldsymbol{\alpha}_i)} e^{-j\psi(\tau_2,\boldsymbol{\alpha}_j)}\, d\tau_1\, d\tau_2 = \delta_{a^2}(1-a^2). \end{aligned} \tag{36}$$

Inserting the above quantities into (27) yields the parameters A and B which are necessary to compute the exact pairwise error probability in (26). We follow the approach used in [6] and apply

the approximation [14]

$$P(\boldsymbol{\alpha}_i \to \boldsymbol{\alpha}_j) \approx Q\left(\sqrt{\frac{\mathcal{E}_b}{N_0} d'^2}\right) \tag{37}$$

where $\mathcal{E}_b$ is the energy per bit, which satisfies $\mathcal{E} = \mathcal{E}_b \log_2 M$, and

$$Q(x) = \frac{1}{\sqrt{2\pi}} \int_x^\infty e^{-u^2/2}\, du. \tag{38}$$

The quantity d'^2 is a normalized equivalent squared Euclidian distance given by

$$d'^2 = \frac{\log_2 M}{\mathcal{E}/N_0} \left(\sqrt{B} - \sqrt{A}\right)^2 \tag{39}$$

which is analogous to the squared Euclidian distance d^2 discussed in detail in [6]. This approximation is valid under the conditions $A \gg 1$, $B \gg 1$, which are satisfied when $\mathcal{E}_b/N_0$ is large.

Unfortunately, the expressions in (27) do not simplify into a form where the behavior of d'^2 is readily apparent. We point out that the leakage factor is present in M_i, M_j, σ^2, and ρ, and that the difference between the two data sequences, $\boldsymbol{\gamma}$, is present in (34). The connection between these terms and d'^2 will be demonstrated in the examples in Section 4.

3.2 Probability of Error

To arrive at the probability of error, we begin from the familiar standpoint of the union bound where

$$P_e \leq \sum_i P(\boldsymbol{\alpha}_i) P_e(\boldsymbol{\alpha}_i) \tag{40}$$

and $P(\boldsymbol{\alpha}_i)$ is the probability that the data sequence $\boldsymbol{\alpha}_i$ is transmitted. The term $P_e(\boldsymbol{\alpha}_i)$ is the probability of error given $\boldsymbol{\alpha}_i$ was transmitted, which is overbounded by

$$P_e(\boldsymbol{\alpha}_i) \leq \sum_{j \neq i} P_e(\boldsymbol{\alpha}_i \to \boldsymbol{\alpha}_j) \tag{41}$$

which uses the pairwise error probability derived above.

Due to the nature of (38), as $\mathcal{E}_b/N_0$ increases, the sum in (41) is dominated by the terms with

the smallest values of $d'(\boldsymbol{\gamma})$. Our task is to find the sequence

$$\boldsymbol{\gamma}_{\text{min}} = \arg\min_{\boldsymbol{\gamma}} d'(\boldsymbol{\gamma}) \tag{42}$$

which in general has a limited number of non-zero coordinates, say R, and we arbitrarily assign the first of these coordinates to be γ_0. For multi-h CPM, the search in (42) must be repeated N_h times to allow each modulation index to coincide with γ_0. The obvious candidates for the search in (42) are the sequences that cause two paths to deviate in the trellis for a limited interval and then merge back together. For the optimal coherent trellis, which has a phase state, the requirement for a merge is

$$\left(\sum_{l=0}^{R-1} k_l \gamma_l\right) \bmod p = 0 \tag{43}$$

which is to say that all the difference coordinates must sum to zero, modulo-2π, when properly scaled by the modulation indexes in (3). For this noncoherent trellis, which does not have a phase state in its $(L+N-1)$-tuple, a merge occurs simply when the coordinates of $\boldsymbol{\gamma}$ are zero for a long enough interval. In general, the duration in which paths are different in this noncoherent trellis is $L+N+R-2$ symbol times. For example, consider a 4-ary 2RC CPM scheme with $\boldsymbol{\gamma}_{\text{ex}} = \cdots, 0, 2, -2, 0, \cdots$ which has $R = 2$. The trellis paths taken by the two data sequences will be different for a span of $2+N$ symbol times. With $M = 4$, there are 18 such pairs of length-2 sequences ($\boldsymbol{\alpha}_i$,$\boldsymbol{\alpha}_j$) that differ by $\pm\boldsymbol{\gamma}_{\text{ex}}$. In general, this number is given by

$$N(\boldsymbol{\gamma}) = 2\prod_{l=0}^{R-1}\left(M - \frac{|\gamma_l|}{2}\right). \tag{44}$$

With the search in (42) complete, we convert the probability of error in (40) to a bit error probability via

$$P_b \approx \frac{N(\boldsymbol{\gamma}_{\text{min}})W(\boldsymbol{\gamma}_{\text{min}})}{N_h \cdot M^R \cdot \log_2 M} Q\left(\sqrt{\frac{\mathcal{E}_b}{N_0} d'^2_{\text{min}}}\right) \tag{45}$$

where $W(\boldsymbol{\gamma}_{\text{min}})$ is the difference, in bits, between the $(\boldsymbol{\alpha}_i, \boldsymbol{\alpha}_j)$ pairs (i.e. the bit error weight), which is a function of the mapping from bits to symbols (typically a Gray code). We assume $P(\boldsymbol{\alpha}_i) = 1/(N_h M^R)$ which is the uniform distribution of all length-R sequences with a particular

alignment to the modulation indexes.

4 Examples

Quaternary 2RC with $h = 1/4$

The first scheme we consider is $M = 4$, 2RC with $h = 1/4$. This CPM scheme was also examined in [2]. The optimal trellis has $S = 16$ states and a minimum squared distance of $d^2_{\text{min}} = 1.33$, which corresponds to $\boldsymbol{\gamma}_{\text{min}} = [\cdots, 0, 2, -2, 0, \cdots]$ where $R = 2$. There are $N(\boldsymbol{\gamma}_{\text{min}}) = 18$ $(\boldsymbol{\alpha}_i, \boldsymbol{\alpha}_j)$ pairs of this type, each with an error weight of 2 bits. The bit error probability of the optimal coherent receiver is given by (45) with d^2_{min} substituted for d'^2_{min}.

For the noncoherent receiver, we select $N = 1$ and $a = 0.9$, which yields a $S = 4$ state trellis. We find that the same difference sequence corresponds to the minimum distance; however, for the purposes of computing A and B we use $\boldsymbol{\gamma}_{\text{min}} = [\cdots, 0, 2, -2, 0]$. This $\boldsymbol{\gamma}_{\text{min}}$ is infinitely long on the left-hand side and ends with one zero coordinate on the right hand side, which corresponds to the trellis paths being different for a total of $L + N + R - 2 = 3$ symbol times. For the parameters required to compute A and B we have

$$M_i = 10\sqrt{\mathcal{E}}, \qquad M_j = (9.40 + j1.20)\sqrt{\mathcal{E}} \tag{46}$$

$$\sigma^2 = 5.26, \qquad \rho = 0.90 + j0.21 \tag{47}$$

where we set the unknown and irrelevant channel phase to $\phi = 0$ for convenience. These parameters yield $A = 7.62\mathcal{E}$ and $B = 12.58\mathcal{E}$ and an equivalent squared distance of $d'^2_{\text{min}} = 1.24$, which is 0.31 dB inferior to that of the optimal coherent receiver. Figure 1 shows P_b for both the coherent and noncoherent receivers, where the 0.31 dB difference in performance is visible. The figure also shows computer simulation data for the noncoherent receiver. The first conclusion we draw from the figure is that the analytical bound and the simulated data show strong agreement as $\mathcal{E}_b/N_0$ increases. In the figure we also show simulations which are based on the noncoherent receivers from Colavolpe and Raheli [2] and Aulin and Sundberg [3] that were discussed in

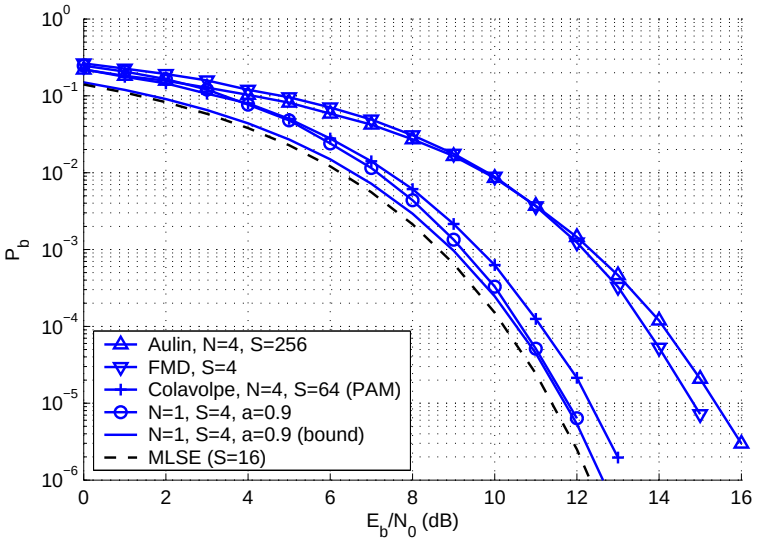

Figure 1: Performance of 4-ary 2RC with $h = 1/4$. The noncoherent receiver with $S = 4$ states is within 0.31 dB of the optimal coherent receiver which has $S = 16$. The performance bound for the noncoherent receiver also shows strong agreement with data from computer simulations. This noncoherent receiver outperforms three other noncoherent schemes (also shown) at a fraction of the complexity of these.

Section 2.3. Also shown are simulations using a simple FM demodulator technique which uses a limiter-discriminator followed by a sequence detector [15]. The second conclusion from Figure 1 is that the noncoherent receiver presented here outperforms the other noncoherent techniques. The $S = 64$ receiver from [2] is the closest in performance with a 1 dB loss with respect to the optimal coherent receiver (this value of $S = 64$ is as presented in [2] using the PAM representation). The 0.31 dB loss of our $S = 4$ receiver is an improvement in both performance and complexity reduction over these other techniques.

It is also interesting to note that if we select $a = 0.99$ we have $d'^2_{\text{min}} = 1.32$, which is within 0.03 dB of the optimal value of $d^2_{\text{min}} = 1.33$. This behavior confirms the intuition which suggests that as $a \rightarrow 1$, the circle in the complex plane in which the correct metric lies has a radius that approaches infinity ($\sqrt{\mathcal{E}}/(1-a)$). Since a circle with an infinite radius has no curvature, a competing metric can have a larger magnitude only if the additive noise moves it beyond the correct metric in the outward direction along the line at angle ϕ. These are exactly the conditions in which errors occur in the coherent receiver, where $\phi = 0$ and metrics are compared on the real line. For a circle of smaller radius, the curvature of the circle allows competing metrics to attain a larger

magnitude with additive noise at other angles in addition to ϕ. This corresponds to a less than optimal equivalent distance when a is not very close to 1. For this CPM scheme, both the coherent and noncoherent receivers have the same minimum distance merge $\boldsymbol{\gamma}_{\text{min}}$ and have trellis paths that differ for 3 symbol times in both cases. With these characteristics in common, it is not surprising that the two distance values converge.

Quaternary 3RC with $h = \{4/16, 5/16\}$

The second scheme we consider is $M = 4$, $3RC$, $h = \{4/16, 5/16\}$. This is the Advanced Range Telemetry (ARTM) Tier II proposed waveform [16]. The optimal receiver has $S = 512$ states and a minimum squared distance of $d^2_{\text{min}} = 1.29$. This distance is for $\boldsymbol{\gamma}_1 = [\cdots, 0, 2, -4, 6, -4, 2, 0, \cdots]$ ($R = 5$) when $h_0 = 4/16$ coincides with γ_0. There are $N(\boldsymbol{\gamma}_1) = 72$ signal pairs of this type, each with an error weight of 7 bits. There is an additional merge $\boldsymbol{\gamma}_2 = [\cdots, 0, 2, -2, 0, 2, -2, 0, \cdots]$, with a squared distance of $d^2(\boldsymbol{\gamma}_2) = 1.66$, which is much more likely to be transmitted ($N(\boldsymbol{\gamma}_2) = 648$) and makes a meaningful contribution to the performance bound for practical values of $\mathcal{E}_b/N_0$. Both of these merges satisfy the condition in (43).

For the noncoherent receiver, we again select $N = 1$ and $a = 0.9$, which this time yields a $S = 16$ state trellis. Here we find that the minimum distance is associated with $\boldsymbol{\gamma}_{\text{min}} = [\cdots, 0, 2, -2, 0, 0]$, which is not itself a merge in the coherent receiver since it does not satisfy (43) (note that we have padded two zeros on the right-hand side of $\boldsymbol{\gamma}_{\text{min}}$ since $L = 3$ in this case). With this merge we have $R = 2$, $N(\boldsymbol{\gamma}_{\text{min}}) = 18$, and an error weight of 2 bits. For the parameters required to compute A and B we have

$$M_i = 10\sqrt{\mathcal{E}}, \qquad M_j = (9.61 + j0.72)\sqrt{\mathcal{E}} \tag{48}$$

$$\sigma^2 = 5.26, \qquad \rho = 0.94 + j0.11 \tag{49}$$

which yield $A = 7.66\mathcal{E}$ and $B = 11.67\mathcal{E}$ and an equivalent squared distance of $d'^2_{\text{min}} = 0.84$. This is 1.85 dB inferior to the optimal coherent receiver. If we select $N = 2$ the distance improves to $d'^2_{\text{min}} = 1.02$, which is only 1 dB inferior but increases the number of states to $S = 64$ (to compute

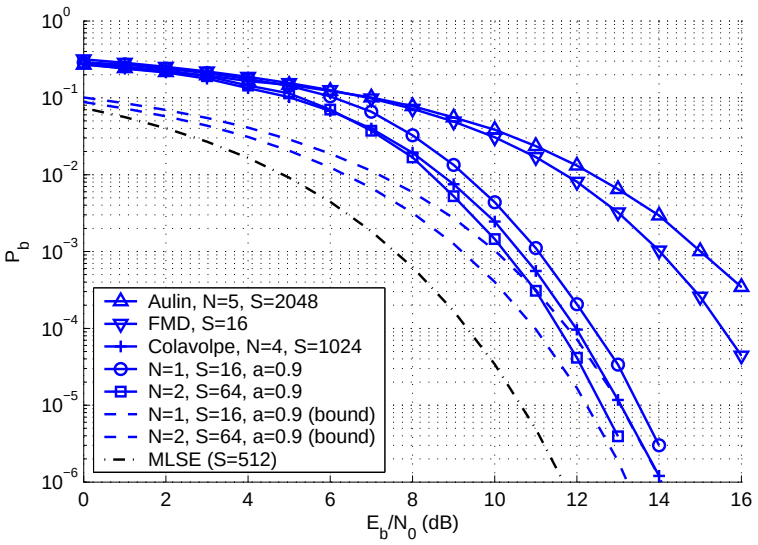

Figure 2: Performance of 4-ary 3RC with $h = \{4/16, 4/16\}$. The noncoherent receiver is simulated with $N = 1$ ($S = 16$) and $N = 2$ ($S = 64$). A performance gain is obtained with the increase in N. There is a slight disparity between the predicted and simulated bit error probabilities from error propagation due to decision feedback. These proposed receivers again outperform existing noncoherent receivers both in complexity and probability of error.

the distance with $N = 2$ we must pad an another zero on the right-hand side of $\boldsymbol{\gamma}_{\text{min}}$). The fact that the performance improves with increasing N is expected since we add another symbol coordinate to the receiver hypothesis and allow more distance to accumulate between competing paths before survivors are declared.

Figure 2 shows P_b for the coherent and for both of these noncoherent configurations ($N = 1$ and $N = 2$) along with simulated data points. The first observation is that the simulated data do not line up exactly with the predicted bound for this scheme. An examination of the actual error events that were encountered in the simulation yields some insight. The error events themselves occur with the expected probability, $Q(\sqrt{d'^2_{\text{min}}\mathcal{E}_b/N_0})18/(2 \cdot 4^2)$, but in many instances they do not resemble $\boldsymbol{\gamma}_{\text{min}}$ or they occur as a $\boldsymbol{\gamma}_{\text{min}}$ sequence that is immediately followed by some other error sequence. The likely cause of this unexpected behavior is error propagation due to decision feedback, which is used to compute (22). In some instances the occurrence of the first error event $\boldsymbol{\gamma}_{\text{min}}$ results in surviving metrics that are "weakened" and are more prone to additional errors in the immediate term. A second and more subtle explanation is linked to the fact that this particular merge is an artifact of the noncoherent trellis and is not a true merge of two CPM signals. Thus,

when this merge defeats the correct path, the metric begins to grow at a different phase angle in the complex plane. In transitioning to the steady-state value at this new angle, the metric passes closer to the origin and opens the possibility that yet another incorrect sequence will defeat $\boldsymbol{\gamma}_{\text{min}}$ and be output by the receiver at traceback time. In such a case the root cause of the error event is $\boldsymbol{\gamma}_{\text{min}}$ but the resulting bit error weight is different than 2 bits. Regardless of the cause, the simulations suggest that the resulting bit error weight is approximately 6 instead of 2. In simulating other CPM schemes (not presented here), similar disparities appear between the predicted and observed bit error probabilities in those cases where the merge in the noncoherent trellis is not a true merge.

Unlike the previous example, increasing a does little to improve d'^2_{min} (in fact, simulations show that the error propagation worsens since the metrics do not "leak" out any of the previous incorrect decisions). This comes as no surprise since the minimum distance merges in the two receivers are entirely different and the trellis paths are separate for 7 symbol times in the coherent receiver and a mere $3 + N$ times in the noncoherent receiver. The only means of improving the distance for this CPM scheme is to increase N, which comes with an M-fold increase in the number of states for each increment. At some point, these increments in N would result in $\boldsymbol{\gamma}_1$ becoming the minimum distance merge, as is the case with the coherent receiver.

Figure 2 also shows simulations for the same lineup of existing noncoherent receivers as the previous example. As before, the receiver in [2] performs the best of these, but requires $S = 1024$ to achieve performance comparable to the $S = 16$ and $S = 64$ receivers proposed here. We again note that the PAM approximation [17] is available to reduce complexity to some degree; but since this approximation is available to all these noncoherent schemes there still remains an inherent complexity and performance advantage for the noncoherent receiver presented here.

5 Conclusion

We have presented a noncoherent receiver for CPM that has characteristics of existing coherent and noncoherent receiver architectures. The receiver achieves some performance gains from its controlled use of a cumulative metric. It also has a parameter analogous to a multi-symbol observation

interval which, when increased, can bring additional performance gains. We have derived an exact expression for the pairwise error probability for this receiver. This expression, or an equivalent Euclidian distance, can be used in a union bound on the bit error probability with strong agreement with computer simulations. There are instances where error propagation, due to the use of decision feedback in the receiver, causes additional errors that are not accounted for in the performance bound. These cases appear to be limited to those where the error merges in the trellis are not true signal merges. This receiver also appears to be robust in phase noise conditions. Overall, the receiver shows promise in providing both performance gains and complexity reduction over existing noncoherent receivers.

REFERENCES

[1] G. Colavolpe and R. Raheli. "Noncoherent sequence detection". *IEEE Transactions on Communications*, 47(9):1376–1385, September 1999.

[2] G. Colavolpe and R. Raheli. "Noncoherent sequence detection of continuous phase modulations". *IEEE Transactions on Communications*, 47(9):1303–1307, September 1999.

[3] T. Aulin and C-E. Sundberg. "Partially coherent detection of digital full response continuous phase modulated signals". *IEEE Transactions on Communications*, 30(5):1096–1117, May 1982.

[4] D. Makrakis and K. Feher. "Multiple differential detection of continuous phase modulated signals". *IEEE Transactions on Communications*, 40(2):186–196, May 1993.

[5] D. Raphaeli. "Noncoherent coded modulation". *IEEE Transactions on Communications*, 44(2):172–183, February 1996.

[6] J. B. Anderson, T. Aulin, C-E. Sundberg. *Digital Phase Modulation*. Plenum Press, New York, 1986.

[7] G. Colavolpe and R. Raheli. "Reduced-complexity detection and phase synchronization of CPM signals". *IEEE Trans. on Commun.*, 45:1070–1079, Sept. 1997.

[8] J. Proakis. *Digital Communications*. McGraw-Hill, New York, 1989.

[9] P. A. Laurent. "Exact and approximate construction of digital phase modulations by superposition of amplitude modulated pulses (AMP)". *IEEE Transactions on Communications*, 34:150–160, February 1986.

[10] U. Mengali and M. Morelli. "Decomposition of M-ary CPM signals into PAM waveforms". *IEEE Transactions on Information Theory*, 41:1265–1275, September 1995.

[11] A. Svensson. "Reduced state sequence detection of partial responce continuous phase modulation". *IEE Proceedings, part I*, 138:256–268, August 1991.

[12] S. Stein. "Unified analysis of certain coherent and noncoherent binary communications systems". *IEEE Transactions on Information Theory*, 10:43–51, January 1964.

[13] J. Marcum. "Tables of Q functions". Technical report, RAND Corp. Rep. M-339, January 1950.

[14] M. Schwartz, W. R. Bennett, S. Stein. *Communications Systems and Techniques*. McGraw-Hill, New York, 1965.

[15] E. Perrins and M. Rice. "Comparison of receivers for multi-h CPM". In *Proceedings of the International Telemetering Conference*, San Diego, CA, October 2002.

[16] M. Geoghegan. "Description and performance results for a multi-h CPM telemetry waveform". In *Proceedings of IEEE MILCOM*, volume 1, pages 353–357, October 2000.

[17] E. Perrins and M. Rice. "PAM decomposition of M-ary multi-h CPM". *submitted for publication in IEEE Transactions on Communications*.